Preprint Manuscript, 6/20/2017
Under review at *European J. Neuroscience*, 6/24/2017

Striatal cholinergic receptor activation causes a rapid, selective, & state-dependent rise in corticostriatal β activity

Benjamin R. Pittman-Polletta[1*†], Allison Quach[2*], Ali I. Mohammed[2], Michael Romano[2], Krishnakanth Kondabolu[2], Nancy J. Kopell[1], Xue Han[2†], Michelle M. McCarthy[1†]

Abstract
Cortico-basal ganglia-thalamic (CBT) β oscillations (15–30 Hz) are elevated in Parkinson's disease and correlated with movement disability. To date, no experimental paradigm outside of loss of dopamine has been able to specifically elevate β oscillations in the CBT loop. Here, we show that activation of striatal cholinergic receptors selectively increases β oscillations in mouse striatum. Furthermore, β expression in primary motor cortex (M1) distinguishes two BG dynamical states. In one, β oscillations increase in both striatum and M1, with partial directed coherence occurring primarily from striatum to M1 and distinguishing between β subbands. In another, M1 is characterized by persistent β-HFO phase-amplitude coupling, and shows no β increase. This suggests: (1) striatal cholinergic tone exerts state-dependent and frequency-selective control over CBT β power and coordination; (2) ongoing rhythmic dynamics can determine whether elevated striatal β oscillations are expressed in M1; (3) altered striatal cholinergic tone differentially modulates distinct β subbands.

[1] *Boston University, Department of Mathematics & Statistics, Boston, MA 02215*
[2] *Boston University, Department of Biomedical Engineering, Boston, MA 02215*
*These authors contributed equally to this work.
†**Corresponding authors**: benpolletta@gmail.com (BRPP), xuehan@bu.edu (XH), mmccart@bu.edu (MMM).

1. Introduction

The striatal cholinergic system is emerging as a key mediator of parkinsonian motor symptoms. Chronic loss of dopamine diminishes M4 autoreceptor functioning on striatal cholinergic interneurons (sChIs), which normally function to regulate release of acetylcholine (ACh) [1]. Increased levels of ACh occur in the striatum of both the 6-OHDA rat model of Parkinson's disease (PD) as well as after acute antagonism of dopamine D2 receptors [2]. Optogenetic activation of striatal cholinergic interneurons (SChIs) promotes parkinsonian-like motor symptoms in normal mice [3], whereas silencing SChIs improves motor symptoms in dopamine depleted parkinsonian mouse models [4]. Furthermore, intra-striatal infusion of cholinergic muscarinic antagonists alleviates parkinsonian motor symptoms [5], and antipsychotic-induced parkinsonism has been recently attributed to SChI activity [6]. Despite the evidence linking the striatal cholinergic system and parkinsonian motor deficits, the neuronal dynamics mediating cholinergic-induced movement disability are unknown. Understanding the neuronal and network mechanisms underlying cholinergic-induced movement disability would provide a framework for identifying likely targets for therapeutic interventions.

A common measure of neuronal dynamics, the local field potential (LFP), shows elevated and coordinated oscillations within the extended β frequency range (8–35 Hz) in cortico-basal ganglia-thalamic (CBT) circuits in PD patients and animal models of PD that correlate with movement disability [7, 8, 9, 10, 11, 12, 13]. To date, no experimental paradigm (pharmacologic or optogenetic) outside of loss of dopamine has been able to elevate oscillations in the CBT loop specifically in the β frequency range. While there is some suggestion that the striatal cholinergic system can modulate β oscillations in CBT circuits, evidence is lacking for specificity of modulation to the β frequency range. Previous studies optogenetically stimulating striatal cholinergic interneurons in normal mice elevated oscillatory power at all frequencies greater than approximately 10 Hz, including both β and broadband γ oscillations [3]. Prior studies with carbachol-induced β oscillations in striatum did not address specificity of elevation to the β frequency range [14]. Additionally, since the recordings were limited to striatum, these studies could not determine more widespread effects of striatal cholinergic modulation within CBT circuits [14]. To determine whether modulations of striatal cholinergic tone are sufficient to elevate and coordinate oscillations specific to the β frequency range in normal, non-parkinsonian CBT circuits, we elevated striatal cholinergic tone with infusions of carbachol while recording LFPs from both striatum and M1. We found that acute increases in striatal cholinergic tone can both selectively increase β oscillations in striatum and M1 as well as increase

coordination between these two regions specifically in the β frequency range. Since the dynamic changes are acute, these findings have the important implication that the mechanism of exaggerated β oscillations in PD may stem from normal physiological processes in CBT circuits, rather than from plastic changes due to the chronic loss of dopamine. This paper presents evidence for the existence of β-generating network mechanisms in normal, non-parkinsonian states within CBT circuits as well as evidence that both the power and coordination of β oscillations can be regulated by striatal cholinergic receptors.

2. Results

To determine how activation of striatal cholinergic receptors affects oscillations in both striatum and the larger CBT loop, we simultaneously recorded LFPs from striatum and M1 while infusing carbachol into the striatum of normal mice (Fig. 1a). In the striatum, carbachol infusion induced frequent bursts of strongly elevated β oscillations, with each burst lasting for hundreds of milliseconds to seconds (Fig. 1a). Consistent with our previous study [14], such bursting was never observed before carbachol infusion.

2.1 Carbachol Infusion Selectively Increases Striatal β Power

Carbachol infusion generated long-lasting increases in oscillatory power, with increases in β power lasting longer than increases in power at other frequencies. To quantify periods of increased band power, we compared 5-minute sliding windows of power to all power pre-infusion ("baseline power") within 7 different frequency bands, δ (1–4 Hz), θ (4–8 Hz), α/low β (8–15 Hz), β (15–30 Hz), γ (30–100 Hz), and high-frequency oscillation (HFO, 120–180 Hz) (Fig. S2. The average duration of increased power was largest for the β band. β power increased over at least one 5 minute period in 10 out of 12 animals, with periods of elevated striatal β power lasting 17.06 ± 5.70 minutes (mean $\pm$ s.d.). These periods began 0.57 ± 1.01 minutes (mean $\pm$ s.d.) after infusion. Furthermore, in 4 of these animals, β remained increased at the end of the recording, 20 minutes post-infusion. In three long recordings (lasting ≥ 40 minutes post-infusion), the increase in striatal β power lasted 21.15 ± 7.29 minutes. While β increases were longer than increases in other frequencies, this difference was not statistically significant. Increases at multiple frequencies may in part be due to longer observation times post-infusion.

To eliminate the effect of longer observation times post-infusion, we examined 2.5-minute "snapshots" of the oscillatory dynamics during both pre- and post-infusion periods, in each band. Examining these snapshots of oscillatory dynamics also allowed us to account for the variable times of expression of carbachol-induced increases in power across animals. More specifically, we compared periods of peak "band power density" (BPD) pre- and post-carbachol.

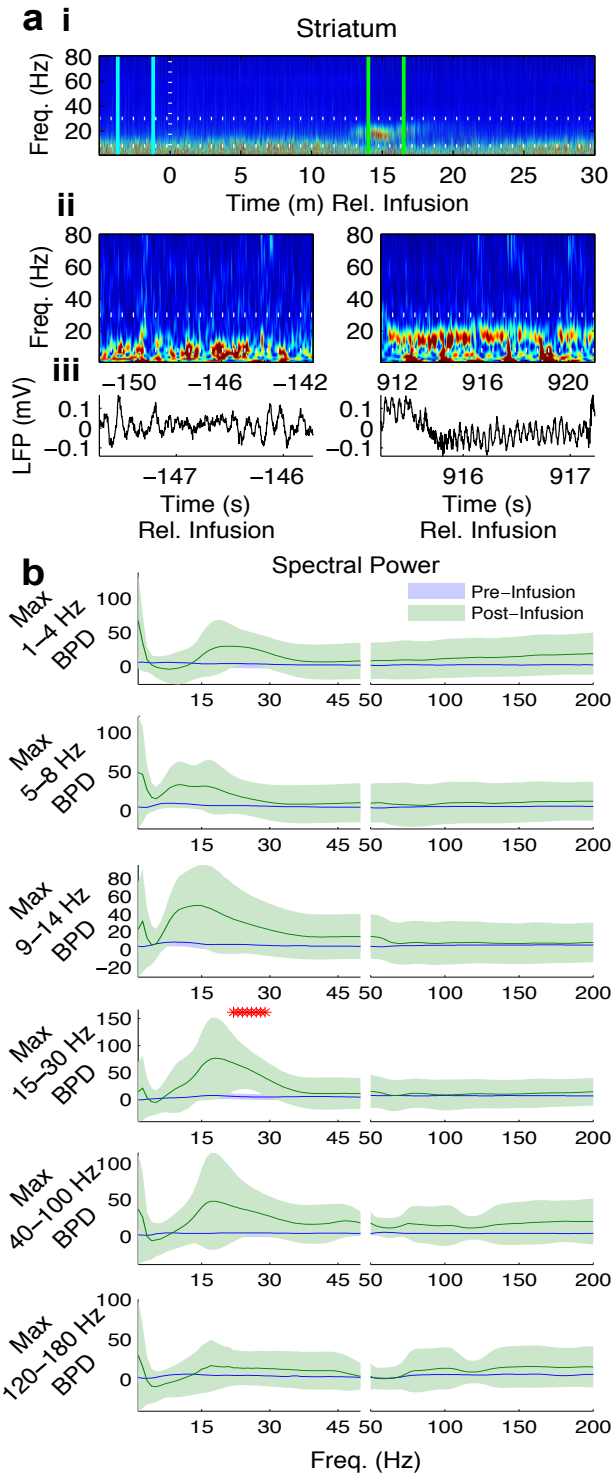

Figure 1. Carbachol selectively increases β oscillations in striatum. (a) Spectrograms of striatal LFP (representative animal). (i) The entire recording. White lines: horizontal, β band; vertical, time of infusion. Green lines: 2.5 mins highest β BPD pre-infusion. Blue lines: 2.5 mins highest β BPD post-infusion. (ii) Ten s in the middle of the period of highest β BPD pre-infusion (left) & post-infusion (right). (iii) Two s of LFP in the middle of the period of highest β BPD pre-infusion (left) & post-infusion (right). (b) Average normalized striatal spectra for periods of highest BPD (mean $\pm$ C.I.). Red stars: significant increases post-infusion.

BPD (the percentage of time when oscillatory power within a specific frequency band is significantly higher than baseline, see Methods and Fig. S2) is a measure that quantifies one of the most salient characteristics of observed increases in band power – namely, an increase in the percentage of time that the band power is higher than "normal" (Fig. 1a).

During the period of highest striatal β BPD post-carbachol, spectral power in striatum increased selectively at high β frequencies (Fig. 1b, row 4). Carbachol induced no other changes in spectral power during this period (Fig. 1b, row 4). Carbachol also failed to induce increases in spectral power at any frequency during periods of highest BPD for non-β bands (Fig. 1b). Interestingly, all periods of highest non-β BPD had distinct, though statistically non-significant, power peaks in the β frequency range. These results extend previous findings [14] by showing that carbachol selectively increases β oscillations in the striatum.

2.2 Carbachol-Induced β Increases are Dichotomously Expressed in M1

In M1, β power changes were inconsistent, with half of mice (n=12 total) exhibiting M1 β power increases post-carbachol co-incident with periods of highest striatal β BPD (Fig. 2). M1 β increases were generally smaller in amplitude than those in the striatum (Fig. 2a), and β power failed to increase post-carbachol at the group level (Fig. S2). To determine the spectral properties associated with the emergence of M1 β, we separated the mice into two subgroups, one containing mice showing M1 β increases at the individual level (M1+, n=6), and one containing mice lacking M1 β increases at the individual level (M1-, n=6).

2.2.1 Subgroup Differences in Spectral Power

In the M1+ subgroup, M1 β power was elevated in the frequency range 19–34 Hz at the subgroup level, while striatal β power was elevated over a narrower β range from 22–28 Hz (Fig. 2b). In contrast, carbachol failed to alter M1 β power at the subgroup level in M1- (Fig. 2b). Interestingly, in the M1- subgroup, striatal β power increased not only in high β (as in M1+) but also in the α band (13–14 Hz and 26–28 Hz, Fig. 2b).

2.2.2 Subgroup Differences in Oscillatory Coordination

In PD, elevation of β power is accompanied by changes in β phase coordination within the CBT loop [7, 15]. In our data, when activation of striatal cholinergic receptors elevates β oscillations in both striatum and M1, it also increases β coordination in corticostriatal circuits. The phase locking value (PLV) between simultaneously recorded LFPs in striatum and M1 was robustly and selectively increased (during periods of highest striatal β BPD) in the higher β frequency range (20–26 Hz) in M1+ but not in M1- (Fig. 2b). We also examined the cross spectrum between M1 and striatum (another measure of rhythmic coordination) and found increases at high β frequencies (27–28 Hz) in M1+ but not in M1- (Fig. 2b).

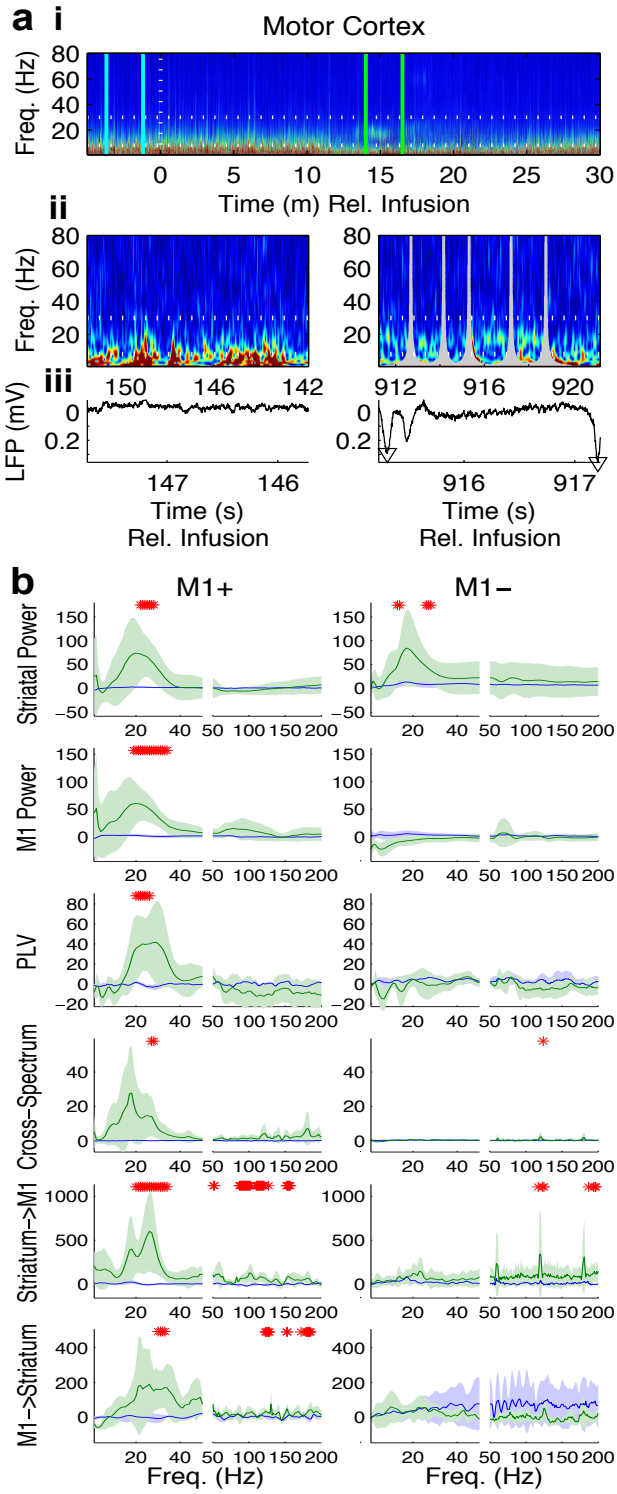

Figure 2. Increases in M1 β power and β coordination are dichotomously expressed after striatal carbachol infusion. (a) Spectrograms of M1 LFP, same animal and format as Fig. 1a. Overlays in Fig. 2aii and triangular symbols in Fig. 2aiii (right panels) demonstrate identification and frequency-dependent removal of "peak" artifacts (see Methods). (b) Average spectral power, PLV, cross spectrum, & partial directed coherence (mean ± C.I.) for groups M1+ and M1-. Red stars: significant increases post-infusion.

The frequency range of these increases in rhythmic coordination is contained in the overlap of the ranges of striatal and M1 β power increases, suggesting increased β phase coordination depends on β power elevations in both regions.

2.3 Carbachol Infusion Alters Information Flow Between Striatum and M1 Differently Within β Subbands

To further characterize the directionality of the elevations in β coordination, we measured partial directed coherence (PDC) between striatal and M1 LFPs during the period of highest striatal BPD. PDC is a measure of how (frequency-specific) fluctuations in one time series predict (frequency-specific) fluctuations in another time series, indicating the flow of information within a given frequency band between structures [16]. In group M1+, PDC analyses revealed that carbachol infusion increased the influence of the striatum on M1 in the β frequency range from approximately 20–34 Hz, and also increased the influence of striatal γ (51–52 & 87–102 Hz) band activity on M1 (Fig. 2b). PDC from M1 to striatum also increased in the β band in M1+, but the increase was restricted to the high β range (30–33 Hz) (Fig. 2b). In group M1-, there was no change in PDC in either direction at frequencies ¡100 Hz. Both groups exhibited changes at frequencies above 100 Hz.

Examining the frequencies at which individual animals exhibited changes in PDC also suggested an association between information flow and β subbands (Fig. 3). Most animals exhibited increases in striatal to M1 PDC at frequencies between 21 and 24 Hz. In contrast, most animals exhibited increases in M1 to striatal PDC at frequencies between 28 and 33 Hz. This suggests that distinct β subbands are differentially modulated following striatal carbachol infusion.

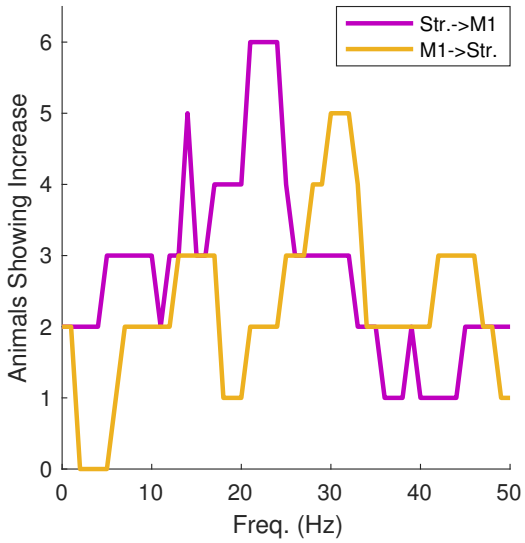

Figure 3. The direction of β PDC increases is frequency-dependent. The number of animals showing carbachol-induced increases in PDC at each frequency between 0 and 50 Hz.

2.4 M1- was Distinguished by Increased β-HFO Phase-Amplitude Coupling

Cross-frequency coupling between brain rhythms within the CBT loop is implicated in the function (and dysfunction) of the motor system, and changes in cross-frequency coupling may characterize behaviorally relevant changes in CBT dynamics [17, 18, 19]. We examined phase-amplitude coupling (PAC), in which the amplitude of a high frequency oscillation exhibits a statistical dependence on the phase of a low frequency oscillation [20, 21], in both striatal and M1 LFPs, pre- and post-infusion, in groups M1+ and M1-. Group M1- showed β-HFO PAC that was clearly absent in group M1+ (Fig. 4). This β phase modulation of HFO power was present during both pre- and post-infusion periods of highest striatal β BPD. This result gives more evidence that groups M1+ and M1- are in distinct dynamical states, even before carbachol infusion occurs. (No clear changes emerged when comparing pre- and post-infusion PAC in either group.)

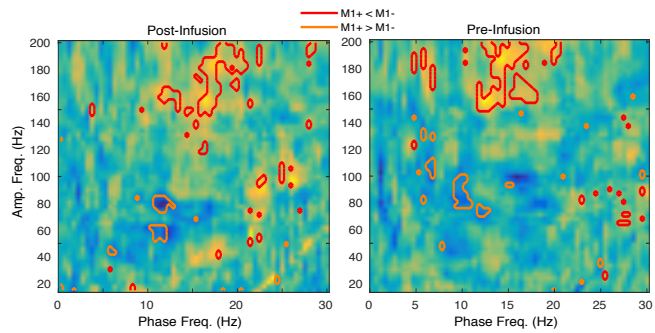

Figure 4. M1 phase-amplitude coupling distinguishes groups M1+ and M1-. The difference in median PAC between groups M1+ and M1- (M1+ subtracted from M1-). Red contours: significantly increased PAC in group M1- as compared to group M1+.

3. Discussion

Infusion of carbachol into the striatum of normal mice brought to light two independent dynamical states in CBT circuits. The first state (M1+) was defined by elevated β frequency oscillations in both striatum and M1, and characterized by: (1) increased coordination between β oscillations in these two structures as measured by PLV and cross-spectral power; and (2) increased information flow between striatum and M1 in the β frequency band. In the second state (M1-), β power was elevated only in striatum, not M1, and β-HFO PAC was robustly present (and increased relative to M1+) both pre- and post-infusion. No changes from baseline in PLV, cross-spectral power, or PDC were noted in state M1-. The existence of the M1- state demonstrates that elevated striatal β may occur independent of elevated M1 β, and that CBT networks can operate in a regime that prohibits exaggerated β oscillations from emerging in M1 when present in striatum. Indeed, such state dependence may explain inconsistent findings on

acute β increases in frontal cortex: experiments on systemic dopamine depletion in anesthetized rats, which failed to increase β power in ECoG recorded from somatomotor cortex [11], may be observations of our state M1-; while experiments in which acute striatal dopamine depletion increased β power in M1 in awake DAT knockout (DAT-KO) mice [22] may be observations of our state M1+.

In contrast to recent experimental work showing that optogenetic stimulation of striatal cholinergic interneurons (sChIs) induces broadband increases in oscillatory power in striatum and M1 [3], the current study shows a selective elevation of power in the β frequency range within corticostriatal circuits, which can be attributed to the stimulation of striatal cholinergic receptors. In group M1+, all significant increases in power, PLV and cross-spectral power, both in striatum and M1, occurred in the β frequency range. Optogenetic stimulation of sChIs increases α, β, and low and high γ power in striatum, and β and low and high γ power in M1 [3]. What could be the source of the sChI-induced elevations in α, low γ, and high γ power, absent in our group M1+? The previous study suggests that sChI-induced high γ is not attributable to activation of striatal cholinergic receptors, since sChI-induced high γ was not reduced by either muscarinic or nicotinic blockade [3]. Since sChIs co-release glutamate with ACh [23], perhaps glutamatergic mechanisms are involved in producing striatal high γ oscillations. Elevated α in striatum, however, may be due to cholinergic mechanisms. Indeed, although α power was not elevated in striatum in group M1+, it was significantly elevated in striatum in group M1-, which indicates that activation of striatal cholinergic receptors can modulate α in a state-depended manner. The source of elevated sChI-induced low γ is unclear, since sChI-induced low γ was diminished following muscarinic blockade. Perhaps the discrepancy between the current pharmacologic and the previous optogenetic study stems from the usage of different ranges for β – part of the range that is significant for β in the current study (30 – 35 Hz) was considered as part of the low γ range in the optogenetic study – or the lower frequency resolution resulting from short trial lengths in the previous study.

The PDC during periods of elevated β in M1+ suggests that much of the flow of information in β (19–34 Hz) is directed from striatum to M1. However, interestingly, part of the higher β band (28–34 Hz) also shows directed information flow from M1 to striatum. Consistent with our results for the higher β band, rats rendered parkinsonian by 6-OHDA lesion show bidirectional Granger causality (GC) between cortex and striatum in the β frequency range with the flow of information predominantly from striatum to cortex [24]. However, since our results showed only unidirectional PDC in the low β range, the bidirectional GC in low β range in the 6-OHDA rats is likely due to mechanisms present in parkinsonian states other than elevated striatal cholinergic tone. Our PDC results may possibly be explained by high β (β_2) being a resonant frequency in CBT circuits, such that amplification and enhanced transmission of the β_2 frequency occurs at multiple sites within the CBT loop. This is consistent with M1 being a suspected generator of β_2 frequencies [25, 26] and with striatum also suspected of generating β over a range of β frequencies [14]. The fact that elevated β_2 oscillations can occur in striatum in the absence of elevated β in M1 (as observed in the M1- group) indicates elevations in striatal β are not dependent on elevated M1 β.

Many of our results suggest a division between high and low β frequencies and further implicate multiple sources of β within the CBT loop. Only high β is coordinated between striatum and M1 as measured by PLV and cross-spectral power. Furthermore, PDC reveals bidirectional communication between striatum and M1 only in the high β (28–34 Hz) frequency range (PDC is unidirectional from striatum to M1 from 19–27 Hz). Additionally, in M1+ PAC between β and HFOs only occurs for low β (less than approximately 20 Hz). These results suggest that there exist at least two frequency ranges within the β band with different properties and perhaps mechanistic sources. This idea is consistent with evidence that suggests low and high β are distinct entities in the parkinsonian basal ganglia, responding differently to dopaminergic therapy and DBS, and potentially correlating with different motor related behavior and motor symptoms in PD [7, 17, 27, 28, 29, 30, 31, 32].

Oscillations at α and low β frequencies may play a mechanistic role in preventing the emergence of elevated M1 β power during states of high striatal cholinergic tone in group M1-. α power (13–14 Hz) is elevated in striatum only in the M1- state, accompanying β elevation in striatum but not in M1. Furthermore, α and low β couple strongly with HFO frequency oscillations in M1 during the M1- state, but not during M1+. Although both the mechanisms of generation and function of HFOs are unknown, it is interesting to note that the HFO frequency that couples to low β (130–200 Hz) is similar to the range of effective frequencies used for deep brain stimulation (DBS) (around 130–185 Hz) for the alleviation of motor symptoms in PD [33]. Perhaps DBS amplifies intrinsic M1 mechanisms that prevent the propagation of elevated β oscillations around the CBT loop. Indeed, HFOs also appear in M1 after severe dopamine depletion in rats, with the amount of β correlating inversely with the amount of HFOs [34], consistent with the idea that the HFOs may offer some protective effect against exaggerated β. Further research into the mechanisms and functions of these HFOs is needed to shed light on these possibilities. Of additional note, the low β-HFO PAC is high both before and after carbachol infusion in state M1-, which not only lends additional evidence to the idea that M1- and M1+ represent two functionally distinct states of CBT dynamics, but also suggests that the dynamical state prior to perturbation by carbachol is a critical regulator of β propagation in CBT circuits. Further characterizing the dynamics present during state M1- may provide additional insight into a normal CBT network state that is capable of preventing the propagation of β oscillations throughout the CBT loop.

The present study shows that β can be acutely elevated in striatum and M1 after stimulation of striatal cholinergic receptors, showing that plastic changes due to chronic loss of dopamine are not required to produce robust β in CBT circuits. Our previous computational modeling work suggests that networks of striatal medium spiny neurons (MSNs) can robustly and reversibly produce β frequency oscillations in response to perturbations that increases the spiking rate of the MSNs, including heightened striatal cholinergic tone and lowered dopaminergic tone [14]. The experimental results reported here support this model of β generation in basal ganglia. Additional support for this model comes from studies showing elevated β oscillations in striatum and M1 after acute loss of dopamine in DAT-KO mice concurrently with parkinsonian motor symptoms [35, 22], suggesting PD β pathology and its associated symptoms may not require long-term plastic changes to basal ganglia structures.

The striatal β model [14] introduces a mechanism capable of producing exaggerated β oscillations acutely. These acute changes in β may coexist with β-producing mechanisms dependent on slow, plastic changes consequent to dopamine depletion, as posited by proposed models of β generation in Parkinson's disease that are dependent on oscillatory dynamics in STN/GPe and GPe/striatal circuits [36, 37, 38, 39, 40]. Similar STN/GPe models may be capable of producing acute increases in β [41]. However, to our knowledge, there is no evidence for acute β increases in STN or GPe following dopamine depletion (or any other experimental manipulation). Indeed there is some evidence that acute β increases are missing in STN following DA depletion: in the 6-OHDA rat model of Parkinson's disease, β oscillations are not elevated in the STN until several days after dopaminergic lesion, and the STN does not show increases in β oscillations after acute disruption of D1 or D2 receptors signaling [11], consistent with the necessity of plastic changes for the production of STN β oscillations. We note that it remains unclear how cholinergic tone affects dopamine in striatum during carbachol infusion [42, 43] and the carbachol-induced β may be working by acutely decreasing dopamine in striatum. However, although recordings from STN were not obtained, it is unlikely that the plastic changes to the STN/GPe circuits due to chronic loss of dopamine which appear necessary for elevated STN β were achieved during the relatively short duration of post-infusion recordings in this study.

A result commonly claimed to refute the possibility of striatal β generation in PD comes from experiments done on MPTP monkeys [44], in which local blockade of projections from striatum to a microregion of GPe failed to abolish β rhythms in that microregion. However, the small proportion of striato-pallidal synapses blocked in these experiments leaves open the possibility that β oscillations propagated from striatum to the blocked portion of GPe through the intact (majority of) projections and pathways connecting these two regions. In particular, while the projections from striatum to GPe are convergent, the loop from STN to GPe and back is highly divergent [45], and may have relayed β from the intact surrounding GPe to the blocked microregion.

Antimuscarinics were a mainstay of therapy for Parkinson's disease until the advent of L-dopa in the 1960s [46] and the current study suggests that the main site of their efficacy may reside in their ability to lower striatal cholinergic tone. However, although striatal neurons may experience hypercholinergia, other cholinergic centers in the brain degenerate in PD, including the basal forebrain cholinergic system, which is the primary source of cholinergic input to the cortex[47]. Thus, although PD patients can experience some relief of symptoms from anticholinergics, the additional hypocholinergia produced in non-striatal sites by systemic anticholinergics in PD patients likely contribute to the limiting side effects of anticholinergic drugs, including cognitive impairment, confusion, memory loss, and nausea [48, 49, 50]. In contrast, targeted striatal anticholinergic interventions alleviate parkinsonian motor symptoms in 6-OHDA mice [4, 5], suggesting that the therapeutic effect of systemic anticholinergics may be due to the lowering of cholinergic tone in striatum. The present study suggests that anticholinergics may exert their beneficial effects in PD by reversing the network dynamics producing exaggerated β oscillations within CBT circuits.

In the present study, we find that activation of striatal cholinergic receptors can selectively elevate the power and coordination of β frequency oscillations in striatum and M1. M1 β oscillations induced by increasing striatal cholinergic tone depend on the dynamic state of the CBT loop prior to and during carbachol infusion. Our results demonstrate a prominent role for striatal cholinergic receptors as state-dependent modulators of β frequency oscillations throughout the CBT loop, and have widespread implications for the importance of these receptors in the control of voluntary movement and its loss in PD.

4. Methods

4.1 Animal Preparations and Recordings

All animal procedures were approved by Boston University's Institutional Animal Care and Use Committee (IACUC), and are in compliance with the National Institutes of Health Guide for the Care and Use of Laboratory Animals. 12 adult mice, C57B6 wild type, or Emx-Arch transgenic mice, both males and females, were used in this study.

Stereotactic surgeries were performed under general anesthesia. Mice were implanted with custom head-plates that allowed access to both striatum and motor cortex. Upon recovery from surgery, mice were head-fixed and recorded from while awake, with glass electrodes (Warner instruments; G100F-4) filled with saline (impedance 1-5 mOhm). Simultaneous recordings were made in the striatum (stereotactic coordinate: AP (anterior posterior) = 0, ML (medial lateral) = 2.5-3 ML, and DV (dorsal ventral) = 2.0–2.5), and the primary motor cortex (AP=-2, ML=1, DV=0.7-1). Local field potential was recorded with a multiclamp 700A amplifier (Molecular

Devices), digitized with a Digidata 1440 (Molecular Devices, Inc.) at 20kHz.

A custom cannula was coupled to the striatal recording electrode with the cannula tip positioned 500μm above the electrode tip. Before carbachol infusion, baseline recordings were made for at least 5 minutes. Carbachol (Sigma C4382) was dissolved in saline at a final concentration of 1μM, and infused at 0.2 μL/min for 5mins (total 1 μL). Recording was performed throughout the infusion period and for at least 12.5 minutes after infusion was started, with the average length of the recordings following the start of infusion being 24.6 $\pm$ 14.6 mins (mean $\pm$ s.d., n = 12 mice).

4.2 Data Analysis

4.2.1 Obtaining Band-Limited Power at Various Frequencies

Power increases observed after carbachol infusion were often bursty rather than continuous. To capture short-duration changes in spectral power, we calculated spectral measures using wavelets. Simultaneously recorded LFPs from each session were first detrended using a 20 second moving average, and then downsampled to 500 Hz sampling rate. They were then convolved with complex Morlet wavelets, spaced every 1 Hz between 1 and 200 Hz. The length of each wavelet was frequency dependent, with the time constant of exponential rolloff of the wavelet spaced linearly between 3 cycles at 1 Hz (for a resulting wavelet length of 3400 ms using eeglab function dftfilt3) and 21 cycles at 200 Hz (for a resulting wavelet length of 120 ms using eeglab function dftfilt3). The modulus of this complex signal provided the instantaneous amplitude or power for each frequency at each time point; its angle provided the instantaneous phase for each frequency at each time point. Power within each of 6 frequency bands – δ (1–4 Hz), θ (4–8 Hz), α/low β (8–15 Hz), β (15–30 Hz), γ (30–100 Hz), and high-frequency oscillation (HFO, 120–180 Hz) – were obtained as the square root of the summed squared power across each frequency range, at each time point.

4.2.2 Identifying Broadband LFP Deflections

Carbachol infusion often produced large peak-like LFP deflections ("peaks", Fig. 3A). These "peaks" had a broadband signature, with the most energy at lower frequencies, and thus complicated our analysis at specific frequency bands. To prevent the spectral signatures of these peaks from biasing our analyses, these "peaks" were first identified and removed before any spectral analysis.

Peak identification was accomplished using one of two methods. For the first method, we first identified putative peak-like deflections using Matlab's findpeaks function, which finds local maxima in the LFP traces that are separated by a minimum time, t_{min}. This argument t_{min} (typically around 1 second) was determined by visual inspection for each recording to ensure that all possible artifactual peaks were selected. We then extracted the LFP waveform from $t_{min}/2$ before to $t_{min}/2$ after the identified putative peaks, and these waveforms were clustered using Matlab's kmeans clustering function. The clusters corresponding to peaks were manually marked for removal. This method was successful in identifying peak-like deflections that exhibited highly stereotypical waveforms.

In the few cases when the first method failed due to peaks being insufficiently stereotypical, a second method was used. In this method, real peaks were selected from putative peaks by manually setting thresholds on "peak prominence", a measure of how large a given peak is relative to the surrounding waveform. Specifically, prominence was calculated by integrating the difference between the height of the putative peak and the value of the local LFP waveform from $t_{min}/2$ before to $t_{min}/2$ after the time of the putative peak. To determine putative peaks, the function findpeaks was used as above, unless peak-like artifacts occurred close to other local maxima in the LFP. In these cases, we noticed that peaks exhibited a particular spectral signature (i.e., their occurrence was accompanied by increases in band power in a specific band, usually δ or θ). Thus, in these cases, we used band-limited power in conjunction with the LFP to identify putative peaks as follows. First, the function findpeaks was used to find maxima in the appropriate band power time series (with the relevant band determined by visual inspection) separated by a time t_{min}. Second, putative peaks were identified as the local LFP maxima located no further in time than t_{jitter} from these maxima in band power. The time t_{jitter} was again determined by visual inspection, and was always smaller than the time $t_{min}/2$ (typically on the order of 10 ms).

4.2.3 Eliminating Effects of Broadband LFP Deflections

After peaks were identified, the spectral parameters possibly affected by these peaks were excluded from both wavelet transforms and band power time series for all subsequent analyses, as follows. The number of data points removed from each time series was proportional to the inverse of the frequency represented by the time series, as seen in Figure 2B. Roughly speaking, for each wavelet component and for each peak, we identified data points at which the magnitude of the Morlet wavelet centered at the peak was greater than 10% of the maximum magnitude of the Morlet wavelet. For example, this would remove all timepoints within 1025 ms of a peak in the 1 Hz time series, all timepoints within 527 ms of a peak in the 2 Hz time series, and all timepoints within 35 ms of a peak in the 200 Hz time series. More exactly, a zero-one vector of peak timepoints (containing ones at each peak and zeros otherwise, so each peak is represented by a one) was convolved with the absolute values of the Morlet wavelets used for spectral analysis described above. The resulting time series were divided by their maxima, and time points at which these normalized time series were greater than 0.1 were set to NaN in all wavelet transforms. The results of these convolutions were also summed over the 6 frequency bands given above; these time series were divided by their maxima, and time points at which the normalized time series were greater than 0.1 were set to NaN in the band power time series. This method successfully removed most of the spectral contamination resulting from peak-like deflections in the LFP.

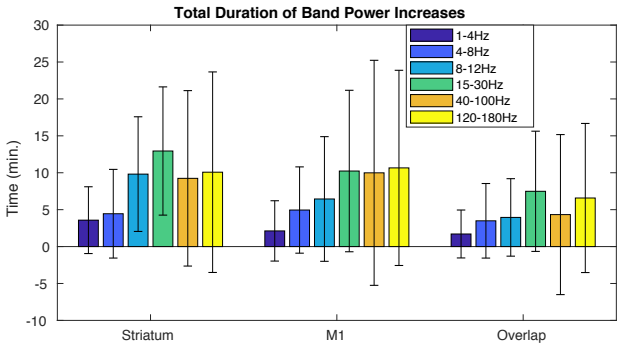

Figure S1. Band power increases relative to baseline in all bands, with beta power increases having the longest duration. Duration of band power increases (mean ± S.E.) is shown for all frequency bands, for the striatal LFP (left), the M1 LFP (middle), and for both LFPs (right).

4.2.4 Duration of Increases in Band-Limited Power

To determine the duration of increases in band power following carbachol infusion, we compared power within sliding 5 min windows (of 300 observations) to power during the pre-infusion baseline period, with one-sided unpaired t-tests at significance level p=0.05. These sliding windows were shifted with a step size of 30 s. Each timepoint was considered to be a timepoint at which β was increased, if it belonged to one sliding window in which power significantly increased from baseline.

4.2.5 Identification of Snapshots of Oscillatory Dynamics Before and After Carbachol Infusion

The duration of recordings following infusion was longer than the duration of recordings before infusion, possibly biasing our calculation of increases in band-limited power (above). In addition, the marked increases in β power visible in wavelet spectrograms (Fig. 1a) occurred at varying times following carbachol infusion. To account for this variability across animals and for the different duration of recordings pre- and post-infusion, we compared "snapshots" of oscillatory dynamics – short periods characteristic of carbachol-induced increases in power at each frequency band – with periods of the same length, selected in the same way, from pre-infusion recordings. More specifically, we utilized a measure called "band power density" (BPD), designed to capture the burstiness of post-carbachol power increases, i.e. to indicate periods of especially dense but not continuous oscillatory activity.

To calculate BPD, we first identified putative timepoints of "high power" in each of the 6 frequency bands – δ (1–4 Hz), θ (5–8 Hz), α/low β (9–14 Hz), β (15–30 Hz), γ (40–100 Hz), and high-frequency oscillation (HFO, 120-180 Hz) –, as timepoints when the z-scored band power at that frequency was higher than 2 standard deviations from the mean over the pre-infusion period. To further eliminate contamination from peaks or smaller LFP deflections that were not removed by the peak detection algorithm described above, we eliminated putative high power timepoints occurring simultaneously with putative high power timepoints in any lower frequency band. The resulting high power timepoints were used to calculate BPD, as the number of high power timepoints per second.

Since carbachol infusion induced power increases happened on a slow time scale of minutes, we used a 2.5 min long sliding window (with steps of 1 second) to identify candidate snapshots of increased oscillatory activity in the striatum. Sliding windows were used to identify the 2.5 min period during which striatal BPD achieved the maximum over the post-infusion period (up to 30 minutes). We used the same method to identify the 2.5 minutes of maximal striatal BPD during the pre-infusion period. Subsequent comparisons are made between the identified 2.5 minute snapshots before and after infusion.

4.2.6 Statistical Comparisons of Pre- and Post-Infusion Power

To avoid fluctuations in lower frequency power from dominating our results (a possibility due to the power-law spectral signature of LFP data), and to allow comparisons between mice, we normalized each wavelet magnitude time series to the mean wavelet magnitude at that frequency during the pre-infusion period. Specifically, we normalized the wavelet magnitude time series as the percent change from mean pre-infusion wavelet magnitude.

Since wavelet transforms are computed using a convolution that essentially "slides" the wavelet time series along the LFP time series, the resulting estimates of power are not independent (i.e., adjacent time points influence each other, with adjacency determined by the length (in cycles) and the frequency of each wavelet – 1700 ms at 1 Hz, 850 ms at 2 Hz, and 60 ms at 200 Hz). To reduce the temporal correlation of the estimates of percent change in power, we divided the 2.5 minute periods analyzed into 150 non-overlapping 1 second long windows. One observation of normalized spectral power was calculated from each window by averaging the percent change in wavelet magnitude over that 1 second.

To determine statistical differences on individual animal level, we used the resulting 150 observations during the two periods, pre and post-infusion, by calculating paired t-tests between the two sets of 150 observations at each frequency. A t-test having a p-value below p = 0.01 for a frequency within the β band (15–30 Hz) indicated a significant change in β power pre- to post-infusion.

For population statistics across mice, average normalized spectral power over the pre- and post-infusion periods was calculated first for each mouse, and then the mean and standard error of normalized power were calculated across mice. A power analysis suggested that for n = 12 and for a standard deviation in normalized spectral power of 30%, an increase in post-infusion normalized spectral power 50% could be detected with a Type II error rate below 10% and Type I error rate below 1%. Thus, we used a significance level of p = 0.01. Mean and 98% confidence intervals of normalized spectral power are plotted for the identified pre- and post-infusion periods, and paired one-sided t-tests across periods at each frequency were used to indicate a significant increase in power

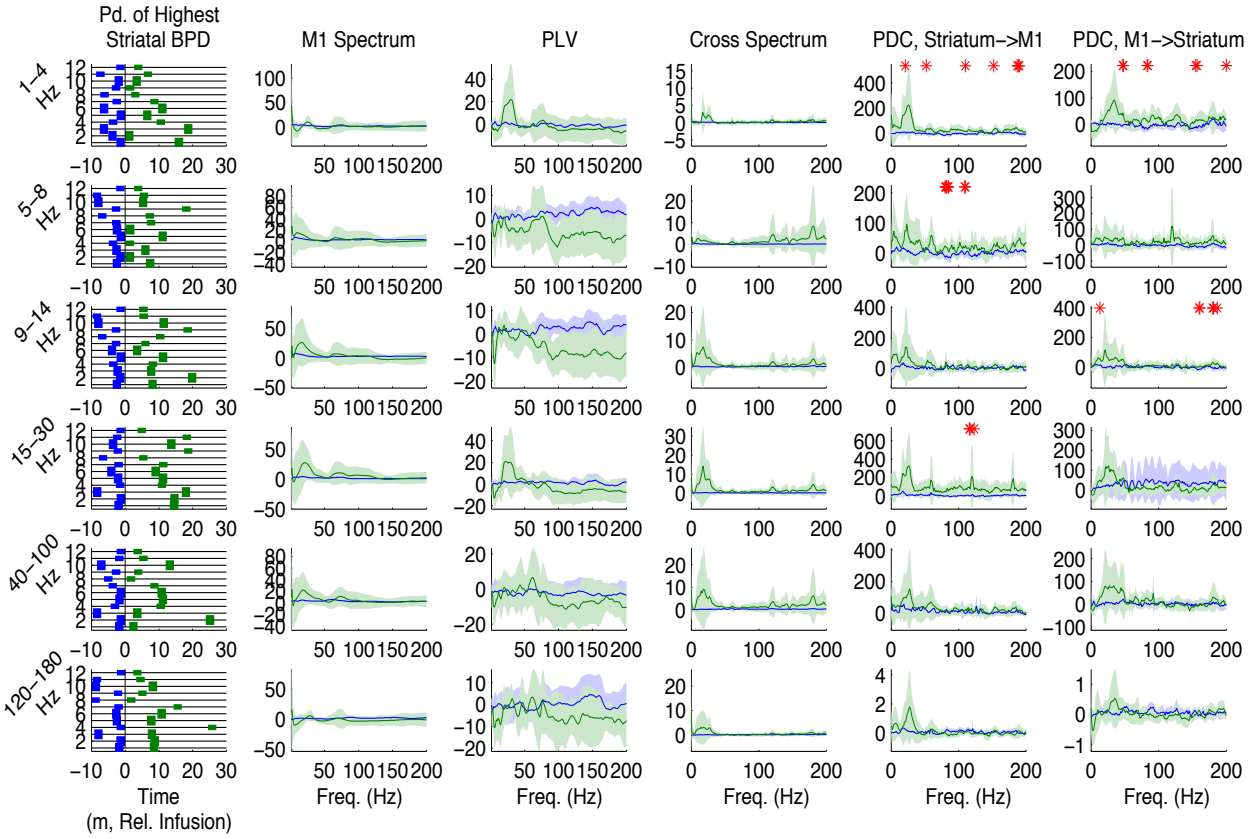

Figure S2. M1 power did not increase post-carbachol during the period of highest BPD for any frequency band. Column 1: The 2.5 min time periods of highest band power density (BPD) for all experiments. Blue bars: period of highest BPD pre-infusion. Green bars: period of highest BPD post-infusion. Thick bars: group M1+. Thin bars: group M1-. Black vertical line: infusion begins. Column 2: Average normalized M1 spectra for periods of highest BPD (mean ± C.I.). Red stars: significant increases post-infusion. Column 3: Average normalized PLV for periods of highest BPD (mean ± C.I.). Red stars: significant increases post-infusion. Column 4: Average normalized cross spectrum for periods of highest BPD (mean ± C.I.). Red stars: significant increases post-infusion. Column 5: Average normalized PDC (striatum→M1) for periods of highest BPD (mean ± C.I.). Red stars: significant increases post-infusion. Column 6: Average normalized PDC (M1→striatum) for periods of highest BPD (mean ± C.I.). Red stars: significant increases post-infusion.

pre- to post-infusion, at level p = 0.01.

4.2.7 Phase-Locking Between M1 and Striatum

To examine phase-locking between M1 and striatum, we computed the magnitude of the mean resultant vector (MRV) of instantaneous phase differences (striatum – M1) for each frequency, for each second, within the identified 2.5 minute analysis window when striatal β BPD was highest, during pre- and post-infusion. First, the instantaneous phase of the wavelet transform in M1 was subtracted from the instantaneous phase of the wavelet transform in striatum, at each frequency and time. The circular mean phase difference at each frequency was then calculated for each second. The magnitude of the MRV provides a measure of the degree of phase consistency or phase-locking between the two recording sites at a particular frequency (phase-locking value, or PLV). As with spectral power, PLV was first normalized as a percentage of baseline (i.e. mean pre-infusion) PLV to allow comparisons across mice.

150 PLV values per period were used to compute differences on an individual level, by computing paired t-tests between periods for a set of 150 observations (pre- and post-infusion) per frequency. Group averaged PLV was then computed first for each mouse (across these 150 observations, and then averaged across mice (n = 12 mice). Paired one-sided t-tests (at significance level p = .01) across periods were used to detect increases in normalized PLV using these 12 observations at each frequency, and are displayed in Fig. S2 alongside the group average and 98% confidence intervals.

4.2.8 Cross-Spectral Power and Partial Directed Coherence

To fit the autoregressive model required for the calculation of cross-spectral power and partial directed coherence (PDC), it was necessary to remove peak artifacts in a way preserving the continuity of the signal in the time domain. Thus, instead of removing timepoints around peak artifacts from the spectral

data in a frequency dependent way, we removed peak artifacts from the time series, by subtracting a suitably scaled average peak waveform from each peak, as follows. First, the set of peak artifacts for each animal was clustered into subsets. Then, a scaled version of the mean peak waveform of each subset was removed from each peak within that subset. Scaling was accomplished by projected the time series around the peak onto the mean peak waveform. The resulting mean peak waveform was windowed and linearly offset, to ensure that the endpoints of the peak-subtracted data matched the endpoints of the raw data, and no discontinuities were introduced by the subtraction.

Following time-domain subtraction of peak artifacts, the pre-infusion baseline periods and the 2.5 min time series during the periods of highest BPD before and after carbachol infusion were divided into 10 s epochs. For each animal, each of these epochs was fit with an autoregressive model, using the MVGC Multivariate Granger Causality Toolbox [16]. These autoregressive models were transformed into frequency-domain cross-spectral and PDC values, also using the MVGC Toolbox. The absolute values of cross-spectral and PDC measures during the 2.5 minutes of highest BPD were normalized by the mean values of these measures during the baseline period for each animal. Normalizations were calculated as the percent change from the baseline mean. At each frequency and for each period (pre- and post-infusion), fifteen normalized values of cross-spectral power and PDC resulted from the 10 s epochs obtained from the period of highest BPD. These 15 values were compared between pre- and post-infusion periods to obtain significant individual-level changes in cross-spectral power and PDC, at significance level $p = 0.01$. The 12 sets of averaged normalized values (one from each animal) at each frequency pre- and post-infusion were compared with paired t-tests at significance level $p = 0.05$ to obtain group-level changes. The group-level difference between post- and pre-infusion cross-spectral power and PDC is plotted in Figure S2.

4.2.9 Phase-Amplitude Coupling

For the calculation of phase-amplitude coupling, we removed peak artifacts in the same way as described above for the fitting of autoregressive models, and divided pre- and post-infusion periods of highest BPD into 10 s epochs. PAC co-modulograms were computed for each epoch, 10 s as follows. For each pair of high-frequency amplitude and low-frequency phase time series (obtained using the wavelet transform as described above), an inverse entropy index [21] was computed. First, a phase-amplitude "distribution" was constructed by: (i) dividing the phase domain $(0, 2\pi]$ into 20 evenly-spaced bins; (ii) averaging the high-frequency amplitudes co-occuring with phases lying in each bin; and (iii) dividing by the sum across bins of these average amplitudes, to yield an empirical marginal distribution of high-frequency amplitude by low-frequency phase. Next, the entropy of this distribution of amplitude by phase – a measure of uniformity across phase – was computed, and normalized to yield a quantity between zero and one. The resulting inverse entropy measure (IE) quantifies the degree of phase-amplitude dependence. An IE of zero indicates no phase-amplitude dependence (a uniform distribution of phase with respect to amplitude). An IE of one is obtained when all the amplitude occurs in a single phase bin. In general, higher IE is awarded to distributions exhibiting a stronger dependence of phase on amplitude, including distributions exhibiting multiple peaks.

For a finite data series, measurements of cross-frequency coupling will always take finite nonzero values, even when no coupling is present in the data. These nonzero values depend in part on the bandwidth, center frequency, and other properties of the observed signals. To remove these non-coupling-related influences, we used surrogate data to estimate "background" values of PAC. These background PAC values were estimated using epoch-shuffled surrogate data: for each channel and each 2.5 min snapshot, all non-simultaneous pairings of 10 s epochs were used to compute non-simultaneous sets of high- and low-frequency time series. These non-simultaneous time series were used to calculate a distribution of surrogate IE values. This distribution was used to z-score the observed IE for each epoch (at each pair of frequencies), yielding a "normalized" measure of significant coupling.

4.2.10 Statistical Comparisons of Groups M1+ and M1-

When comparing within and across subgroups M1+ and M1-, we performed t-tests of the 6 average normalized values of each measure (per group and per period) at each frequency. A power analysis suggested that for $n = 6$ and for a standard deviation in normalized spectral power of 30%, an increase in post-infusion normalized spectral power of 50% could be detected with a Type II error rate below 20% and a Type I error rate below 5%. Thus, we used a significance level of $p = 0.05$. Mean and 90% confidence intervals of normalized spectral power are plotted for the identified pre- and post-infusion periods, and paired one-sided t-tests across periods at each frequency were used to indicate a significant increase in power pre- to post-infusion, at level $p = 0.05$. For comparisons of PAC between groups, the median PAC across epochs was computed for each animal, and the 12 resulting sets of averaged z-scored values (one from each animal) at each frequency pair were compared between groups M1+ and M1-, with ranksum tests at significance level $p = 0.05$ (since PAC measures are not approximately normal, even after z-scoring).

References

[1] J. Ding, J. N. Guzman, T. Tkatch, S. Chen, J. A. Goldberg, P. J. Ebert, P. Levitt, C. J. Wilson, H. E. Hamm, and D. J. Surmeier. Rgs4-dependent attenuation of m4 autoreceptor function in striatal cholinergic interneurons following dopamine depletion. *Nat Neurosci*, 9(6):832–42, 2006.

[2] Y. Ikarashi, A. Takahashi, H. Ishimaru, T. Arai, and Y. Maruyama. Regulation of dopamine d1 and d2 receptors on striatal acetylcholine release in rats. *Brain Res Bull*, 43(1):107–15, 1997.

[3] K. Kondabolu, E. A. Roberts, M. Bucklin, M. M. McCarthy, N. Kopell, and X. Han. Striatal cholinergic interneurons generate beta and gamma oscillations in the corticostriatal circuit and produce motor deficits. *Proc Natl Acad Sci U S A*, 2016.

[4] N. Maurice, M. Liberge, F. Jaouen, S. Ztaou, M. Hanini, J. Camon, K. Deisseroth, M. Amalric, L. Kerkerian-Le Goff, and C. Beurrier. Striatal cholinergic interneurons control motor behavior and basal ganglia function in experimental parkinsonism. *Cell Rep*, 13(4):657–66, 2015.

[5] S. Ztaou, N. Maurice, J. Camon, G. Guiraudie-Capraz, L. Kerkerian-Le Goff, C. Beurrier, M. Liberge, and M. Amalric. Involvement of striatal cholinergic interneurons and m1 and m4 muscarinic receptors in motor symptoms of parkinson's disease. *J Neurosci*, 36(35):9161–72, 2016.

[6] G. Kharkwal, K. Brami-Cherrier, J. E. Lizardi-Ortiz, A. B. Nelson, M. Ramos, D. Del Barrio, D. Sulzer, A. C. Kreitzer, and E. Borrelli. Parkinsonism driven by antipsychotics originates from dopaminergic control of striatal cholinergic interneurons. *Neuron*, 91(1):67–78, 2016.

[7] E. Stein and I. Bar-Gad. beta oscillations in the cortico-basal ganglia loop during parkinsonism. *Exp Neurol*, 245:52–9, 2013.

[8] A. A. Kuhn, A. Tsui, T. Aziz, N. Ray, C. Brucke, A. Kupsch, G. H. Schneider, and P. Brown. Pathological synchronisation in the subthalamic nucleus of patients with parkinson's disease relates to both bradykinesia and rigidity. *Exp Neurol*, 215(2):380–7, 2009.

[9] A. A. Kuhn, F. Kempf, C. Brucke, L. Gaynor Doyle, I. Martinez-Torres, A. Pogosyan, T. Trottenberg, A. Kupsch, G. H. Schneider, M. I. Hariz, W. Vandenberghe, B. Nuttin, and P. Brown. High-frequency stimulation of the subthalamic nucleus suppresses oscillatory beta activity in patients with parkinson's disease in parallel with improvement in motor performance. *J Neurosci*, 28(24):6165–73, 2008.

[10] A. A. Kuhn, A. Kupsch, G. H. Schneider, and P. Brown. Reduction in subthalamic 8-35 hz oscillatory activity correlates with clinical improvement in parkinson's disease. *Eur J Neurosci*, 23(7):1956–60, 2006.

[11] N. Mallet, A. Pogosyan, A. Sharott, J. Csicsvari, J. P. Bolam, P. Brown, and P. J. Magill. Disrupted dopamine transmission and the emergence of exaggerated beta oscillations in subthalamic nucleus and cerebral cortex. *J Neurosci*, 28(18):4795–806, 2008.

[12] A. Sharott, P. J. Magill, D. Harnack, A. Kupsch, W. Meissner, and P. Brown. Dopamine depletion increases the power and coherence of beta-oscillations in the cerebral cortex and subthalamic nucleus of the awake rat. *Eur J Neurosci*, 21(5):1413–22, 2005.

[13] N. Mallet, A. Pogosyan, L. F. Marton, J. P. Bolam, P. Brown, and P. J. Magill. Parkinsonian beta oscillations in the external globus pallidus and their relationship with subthalamic nucleus activity. *J Neurosci*, 28(52):14245–58, 2008.

[14] M. M. McCarthy, C. Moore-Kochlacs, X. Gu, E. S. Boyden, X. Han, and N. Kopell. Striatal origin of the pathologic beta oscillations in parkinson's disease. *Proc Natl Acad Sci U S A*, 108(28):11620–5, 2011.

[15] Hayriye Cagnan, Eugene Paul Duff, and Peter Brown. The relative phases of basal ganglia activities dynamically shape effective connectivity in parkinson's disease. *Brain*, 138(6):1667–1678, 2015.

[16] Lionel Barnett and Anil K Seth. The mvgc multivariate granger causality toolbox: a new approach to granger-causal inference. *Journal of neuroscience methods*, 223:50–68, 2014.

[17] J. Lopez-Azcarate, M. Tainta, M. C. Rodriguez-Oroz, M. Valencia, R. Gonzalez, J. Guridi, J. Iriarte, J. A. Obeso, J. Artieda, and M. Alegre. Coupling between beta and high-frequency activity in the human subthalamic nucleus may be a pathophysiological mechanism in parkinson's disease. *J Neurosci*, 30(19):6667–77, 2010.

[18] Jon López-Azcárate, María Jesús Nicolás, Ivan Cordon, Manuel Alegre, Miguel Valencia, and Julio Artieda. Delta-mediated cross-frequency coupling organizes oscillatory activity across the rat cortico-basal ganglia network. *Frontiers in neural circuits*, 7, 2013.

[19] Constantin von Nicolai, Gerhard Engler, Andrew Sharott, Andreas K Engel, Christian K Moll, and Markus Siegel. Corticostriatal coordination through coherent phase-amplitude coupling. *Journal of Neuroscience*, 34(17):5938–5948, 2014.

[20] Ryan T Canolty and Robert T Knight. The functional role of cross-frequency coupling. *Trends in Cognitive Sciences*, 14(11):506–515, 2010.

[21] Benjamin Pittman-Polletta, Wan-Hsin Hsieh, Satvinder Kaur, Men-Tzung Lo, and Kun Hu. Detecting phase-amplitude coupling with high frequency resolution using adaptive decompositions. *Journal of neuroscience methods*, 226:15–32, 2014.

[22] R. M. Costa, S. C. Lin, T. D. Sotnikova, M. Cyr, R. R. Gainetdinov, M. G. Caron, and M. A. Nicolelis. Rapid alterations in corticostriatal ensemble coordination during acute dopamine-dependent motor dysfunction. *Neuron*, 52(2):359–69, 2006.

[23] M. J. Higley, A. H. Gittis, I. A. Oldenburg, N. Balthasar, R. P. Seal, R. H. Edwards, B. B. Lowell, A. C. Kreitzer, and B. L. Sabatini. Cholinergic interneurons mediate fast vglut3-dependent glutamatergic transmission in the striatum. *PLoS One*, 6(4):e19155, 2011.

[24] J. J. Belic, P. Halje, U. Richter, P. Petersson, and J. Hellgren Kotaleski. Untangling cortico-striatal connectivity

and cross-frequency coupling in l-dopa-induced dyskinesia. *Front Syst Neurosci*, 10:26, 2016.

[25] N. Yamawaki, I. M. Stanford, S. D. Hall, and G. L. Woodhall. Pharmacologically induced and stimulus evoked rhythmic neuronal oscillatory activity in the primary motor cortex in vitro. *Neuroscience*, 151(2):386–95, 2008.

[26] M. G. Lacey, G. Gooding-Williams, E. J. Prokic, N. Yamawaki, S. D. Hall, I. M. Stanford, and G. L. Woodhall. Spike firing and ipsps in layer v pyramidal neurons during beta oscillations in rat primary motor cortex (m1) in vitro. *PLoS One*, 9(1):e85109, 2014.

[27] J. B. Toledo, J. Lopez-Azcarate, D. Garcia-Garcia, J. Guridi, M. Valencia, J. Artieda, J. Obeso, M. Alegre, and M. Rodriguez-Oroz. High beta activity in the subthalamic nucleus and freezing of gait in parkinson's disease. *Neurobiol Dis*, 64:60–5, 2014.

[28] A. Priori, G. Foffani, A. Pesenti, F. Tamma, A. M. Bianchi, M. Pellegrini, M. Locatelli, K. A. Moxon, and R. M. Villani. Rhythm-specific pharmacological modulation of subthalamic activity in parkinson's disease. *Exp Neurol*, 189(2):369–79, 2004.

[29] G. Foffani, A. M. Bianchi, G. Baselli, and A. Priori. Movement-related frequency modulation of beta oscillatory activity in the human subthalamic nucleus. *J Physiol*, 568(Pt 2):699–711, 2005.

[30] Z. Blumenfeld, M. M. Koop, T. E. Prieto, L. A. Shreve, A. Velisar, E. J. Quinn, M. H. Trager, and H. Bronte-Stewart. Sixty-hertz stimulation improves bradykinesia and amplifies subthalamic low-frequency oscillations. *Mov Disord*, 32(1):80–88, 2017.

[31] A. Oswal, M. Beudel, L. Zrinzo, P. Limousin, M. Hariz, T. Foltynie, V. Litvak, and P. Brown. Deep brain stimulation modulates synchrony within spatially and spectrally distinct resting state networks in parkinson's disease. *Brain*, 139(Pt 5):1482–96, 2016.

[32] S. Marceglia, M. Fiorio, G. Foffani, S. Mrakic-Sposta, M. Tiriticco, M. Locatelli, E. Caputo, M. Tinazzi, and A. Priori. Modulation of beta oscillations in the subthalamic area during action observation in parkinson's disease. *Neuroscience*, 161(4):1027–36, 2009.

[33] A. M. Kuncel and W. M. Grill. Selection of stimulus parameters for deep brain stimulation. *Clin Neurophysiol*, 115(11):2431–41, 2004.

[34] I. Brys, J. Nunes, and R. Fuentes. Motor deficits and beta oscillations are dissociable in an alpha-synuclein model of parkinson's disease. *Eur J Neurosci*, 2017.

[35] R. Fuentes, P. Petersson, W. B. Siesser, M. G. Caron, and M. A. Nicolelis. Spinal cord stimulation restores locomotion in animal models of parkinson's disease. *Science*, 323(5921):1578–82, 2009.

[36] A. J. Holgado, J. R. Terry, and R. Bogacz. Conditions for the generation of beta oscillations in the subthalamic nucleus-globus pallidus network. *J Neurosci*, 30(37):12340–52, 2010.

[37] V. L. Corbit, T. C. Whalen, K. T. Zitelli, S. Y. Crilly, J. E. Rubin, and A. H. Gittis. Pallidostriatal projections promote beta oscillations in a dopamine-depleted biophysical network model. *J Neurosci*, 36(20):5556–71, 2016.

[38] O. Shouno, Y. Tachibana, A. Nambu, and K. Doya. Computational model of recurrent subthalamo-pallidal circuit for generation of parkinsonian oscillations. *Front Neuroanat*, 11:21, 2017.

[39] David Terman, Jonathan E Rubin, AC Yew, and CJ Wilson. Activity patterns in a model for the subthalamopallidal network of the basal ganglia. *Journal of Neuroscience*, 22(7):2963–2976, 2002.

[40] Jonathan E Rubin and David Terman. High frequency stimulation of the subthalamic nucleus eliminates pathological thalamic rhythmicity in a computational model. *Journal of computational neuroscience*, 16(3):211–235, 2004.

[41] Arvind Kumar, Stefano Cardanobile, Stefan Rotter, and Ad Aertsen. The role of inhibition in generating and controlling parkinson's disease oscillations in the basal ganglia. *Frontiers in Systems Neuroscience*, 5:86, 2011.

[42] M. E. Rice, J. C. Patel, and S. J. Cragg. Dopamine release in the basal ganglia. *Neuroscience*, 198:112–37, 2011.

[43] S. Threlfell, T. Lalic, N. J. Platt, K. A. Jennings, K. Deisseroth, and S. J. Cragg. Striatal dopamine release is triggered by synchronized activity in cholinergic interneurons. *Neuron*, 75(1):58–64, 2012.

[44] Yoshihisa Tachibana, Hirokazu Iwamuro, Hitoshi Kita, Masahiko Takada, and Atsushi Nambu. Subthalamo-pallidal interactions underlying parkinsonian neuronal oscillations in the primate basal ganglia. *European Journal of Neuroscience*, 34(9):1470–1484, 2011.

[45] Suzanne N Haber. *Integrative Networks Across Basal Ganglia Circuits-Chapter 24*. Elsevier Science & Technology, 2010.

[46] A. Pisani, G. Bernardi, J. Ding, and D. J. Surmeier. Re-emergence of striatal cholinergic interneurons in movement disorders. *Trends Neurosci*, 30(10):545–53, 2007.

[47] N. I. Bohnen and R. L. Albin. The cholinergic system and parkinson disease. *Behav Brain Res*, 221(2):564–73, 2011.

[48] S. H. Fox. Non-dopaminergic treatments for motor control in parkinson's disease. *Drugs*, 73(13):1405–15, 2013.

[49] C. J. Langmead, J. Watson, and C. Reavill. Muscarinic acetylcholine receptors as cns drug targets. *Pharmacol Ther*, 117(2):232–43, 2008.

[50] A. Lees. Alternatives to levodopa in the initial treatment of early parkinson's disease. *Drugs Aging*, 22(9):731–40, 2005.